Available online at www.sciencedirect.com

ScienceDirect

Geochimica et Cosmochimica Acta 208 (2017) 368–380

Geochimica et Cosmochimica Acta

www.elsevier.com/locate/gca

Coupled extremely light Ca and Fe isotopes in peridotites

Xinmiao Zhao [a,*,1], Zhaofeng Zhang [b,*,1], Shichun Huang [c,*], Yufei Liu [b], Xin Li [b], Hongfu Zhang [a,d]

[a] State Key Laboratory of Lithospheric Evolution, Institute of Geology and Geophysics, Chinese Academy of Sciences, Beijing 100029, China
[b] State Key Laboratory of Isotope Geochemistry, Guangzhou Institute of Geochemistry, Chinese Academy of Sciences, Guangzhou 510640, China
[c] Department of Geoscience, University of Nevada, Las Vegas, NV 89154, USA
[d] State Key Laboratory of Continental Dynamics, Department of Geology, Northwest University, Xi'an 710069, China

Received 10 October 2016; accepted in revised form 21 March 2017; Available online 31 March 2017

Abstract

Large metal stable isotopic variations have been observed in both extraterrestrial and terrestrial samples. For example, Ca exhibits large mass-dependent isotopic variation in terrestrial igneous rocks and mantle minerals (on the order of ~2‰ variation in $^{44}Ca/^{40}Ca$). A thorough assessment and understanding of such isotopic variations in peridotites provides important constraints on the evolution and compositon of the Earth's mantle. In order to better understand the Ca and Fe isotopic variations in terrestrial silicate rocks, we report Ca isotopic compositions in a set of peridotitic xenoliths from North China Craton (NCC), which have been studied for Fe isotopes. These NCC peridotites have large Ca and Fe isotopic variations, with $\delta^{44/40}Ca$ ranging from −0.08 to 0.92 (delta value relative to SRM915a) and $\delta^{57/54}Fe$ (delta value relative to IRMM-014) ranging from −0.61 to 0.16, and these isotopic variations are correlated with large Mg# (100 × Mg/(Mg + Fe) molar ratio) variation, ranging from 80 to 90. Importantly, NCC Fe-rich peridotites have the lowest $^{44}Ca/^{40}Ca$ and $^{57}Fe/^{54}Fe$ ratios in all terrestrial silicate rocks. In contrast, although ureilites, mantle rocks from a now broken differentiated asteroid(s), have large Mg# variation, from 70 to 92, they have very limited $\delta^{57}Fe/^{54}Fe$ variation (0.03–0.21, delta value relative to IRMM-014). Our model calculations show that the coupled extremely light Ca-Fe isotopic signatures in NCC Fe-rich peridotites most likely reflect kinetic isotopic fractionation during melt-peridotite reaction on a timescale of several to 10^4 years. In addition, our new data and compiled literature data show a possible compositional effect on the inter-mineral Ca isotopic fractionation between co-existing clinopyroxene and orthopyroxene pairs.

Keywords: Ca isotopes; Fe-rich peridotites; Melt percolation; Lithospheric mantle; North China Craton

1. INTRODUCTION

Calcium is the fifth most abundant element in the Earth. It has six stable isotopes, ranging from mass 40 to 48, and the third largest relative mass difference ($\Delta m/m = 20\%$), which make Ca an important geochemical and cosmochemical tracer (DePaolo, 2004). For example, the Ca cycle is closely coupled to the C cycle in the Earth (DePaolo, 2004; Fantle and Tipper, 2014). In cosmochemistry, comparison of the Ca isotopic compositions of the Earth and meteorites provides important constraints on the formation and evolution of the early Solar System (Clayton et al., 1988; Simon and DePaolo, 2010; Valdes et al., 2014; Huang and Jacobsen, 2017). There is large mass-dependent Ca isotopic variation, measured as $\delta^{44/40}Ca$ relative to a standard sample, in silicate rocks: ~2‰ in terrestrial silicate rocks

* Corresponding authors.
E-mail addresses: xinmiao312@mail.iggcas.ac.cn (X. Zhao), zfzhang@gig.ac.cn (Z. Zhang), shichun.huang@unlv.edu (S. Huang).
[1] These authors contributed equally to this work.

http://dx.doi.org/10.1016/j.gca.2017.03.024
0016-7037/

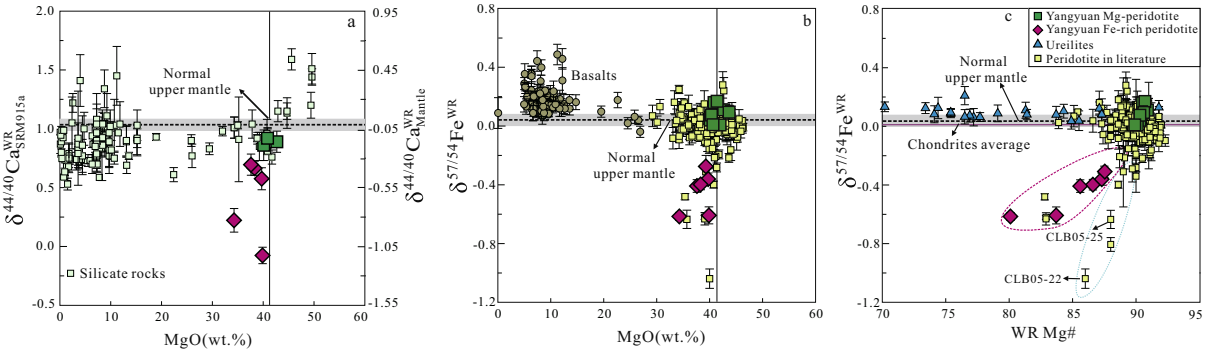

Fig. 1. Plots of whole-rock MgO contents against $\delta^{44/40}$Ca (a) and $\delta^{57/54}$Fe (b) for Yangyuan peridotite xenoliths and silicate rocks. Plot of Mg# vs. $\delta^{57/54}$Fe (c) for Yangyuan peridotites, global peridotites and ureilites. The horizontal dashed line and grey band in panel a represents the suggested upper mantle Ca isotopic composition ($\delta^{44/40}$Ca = 1.05 ± 0.04, Huang et al., 2010a) at MgO = 41.4 wt.% (McDonough, 1990). The horizontal dashed line in panel b represents the suggested upper mantle Fe isotopic composition ($\delta^{57/54}$Fe = 0.04 ± 0.04, Weyer and Ionov, 2007; Craddock et al., 2013) at MgO = 41.4 wt.% (McDonough, 1990). The horizontal purple solid line in panel c represents average chondritic value ($\delta^{57/54}$Fe = 0.01 ± 0.01, Craddock et al., 2013), and the horizontal dashed line in panel c represents the suggested upper mantle Fe isotopic composition ($\delta^{57/54}$Fe = 0.04 ± 0.04, Weyer and Ionov, 2007; Craddock et al., 2013). $\delta^{44/40}$Ca data for Yangyuan peridotites are from Table 1. $\delta^{57/54}$Fe data for Yangyuan peridotites are from Zhao et al. (2015). $\delta^{57/54}$Fe data for ureilites in panel c are from Barrat et al. (2015). See dataset S1 for literature data sources.

compared to ~3‰ in carbonates (Fig. 1; Fantle and Tipper, 2014). What caused such large $\delta^{44/40}$Ca variation in terrestrial silicate rocks? Possible mechanisms include: (a) intermineral isotopic fractionation controlled by mineral structures (Young et al., 2009, 2015; Huang et al., 2010a; Williams and Bizimis, 2014; Kang et al., 2016; Feng et al., 2014); (b) exotic materials such as recycled ancient carbonates in the mantle source (Huang et al., 2011a); (c) kinetic isotopic fractionation effects (Weyer and Ionov, 2007; Dauphas et al., 2010; Teng et al., 2011; Poitrasson et al., 2013; Zambardi et al., 2014; Oeser et al., 2015; Sio and Dauphas, 2017); and (d) partial melting (Weyer and Ionov, 2007; Poitrasson et al., 2013; Kang et al., 2016; Zhong et al., 2017). In order to better constrain and understand the Ca isotopic variation in the mantle, we report Ca isotopic compositions in a series of peridotitic xenoliths from North China Craton (NCC). These peridotites show large $\delta^{44/40}$Ca variation (~1‰), ranging from typical upper mantle-like value (0.92) to −0.08 on the SRM 915a scale, the lowest value ever reported for terrestrial silicate rocks (Fig. 1). Together with published Fe isotopic data (Zhao et al., 2015), we identify a positive correlation between $\delta^{44/40}$Ca and $\delta^{57/54}$Fe in these NCC peridotites. Model calculations show that kinetic isotopic fractionation caused by diffusion, probably during mantle metasomatism, is responsible for the coupled, extremely light Ca and Fe isotopic compositions in these NCC peridotites.

2. SAMPLES STUDIED

Peridotite xenoliths are lithospheric mantle fragments brought to the surface via volcanic eruption, and they provide first-hand information of the isotopic compositions of the Earth's mantle. We study the Ca isotopic variations in a set of NCC peridotitic xenoliths, whose Mg# ranges from 80 to 90, which cover almost the whole Mg# variation in terrestrial peridotites. The studied peridotitic xenoliths were collected from Cenozoic alkali basalts at Yangyuan in the Central Zone of the NCC (Liu et al., 1992). The NCC geological background and the petrology, major and trace element compositions, and Fe isotope compositions of these samples have been reported by Zhao et al. (2015). Here is a short summary.

The studied Yangyuan peridotitic xenoliths are spinel-facies nodules, and two suites of mantle xenoliths (magnesium-peridotites and Fe-rich peridotites) are identified based on petrographic observations and geochemical compositions. The Yangyuan magnesium-peridotites are similar to typical mantle peridotites hosted in basalts from other localities worldwide: Their Mg# range from 89.8 to 90.9, and total FeO contents are between 8.3 and 8.9 wt.%. They are medium- to coarse-grained, and have protogranular microstructures. They contain variable proportions of olivine, orthoyroxene, clinopyroxene and Cr-spinel, and usually do not contain volatile-bearing accessory minerals such as phlogopite and amphibole. Their Al_2O_3 contents range from 2.0 to 3.5 wt.%, and their clinopyroxene REE patters range from slightly LREE-depleted to LREE-enriched, reflecting a low degree melt extraction overprinted by later metasomtism. Their Fe isotopic compositions are similar to typical mantle value, with $\delta^{57/54}$Fe, where $\delta^{57/54}Fe = [(^{57}Fe/^{54}Fe)_{sample}/(^{57}Fe/^{54}Fe)_{IRMM\text{-}014} - 1] \times 1000$, ranging from 0.01 to 0.17.

In contrast, the Fe-rich peridotites represent a compositional and isotopic endmember of global peridotites. Specifically, they define the low Mg# end of the global peridotite spectrum, ranging from 80.1 to 87.5. To the best of our knowledge, they are the lowest Mg# ever reported for terrestrial peridotites (Fig. 1). Petrological and geochemical data argue against a cumulative origin for the Yangyuan Fe-rich peridoties as evidenced by strain and deformation such as kink banding in coarse olivine, whereas olivines in cumulates are not strained (Fig. 2 and supplementary Fig. 2 of Zhao et al., 2015). Based on detailed petrological and geochemical studies, Zhao et al. (2015) have shown that Yangyuan Fe-rich peridotites were formed by

melt-peridotite reaction. Yangyuan Fe-rich peridotites display several stages of orthopyroxene replacement, from nearly intact orthopyroxene grains with rare sieve-textured clinopyroxene at rims to resorbed orthopyroxene relics inside newly formed sieve textured clinopyroxene and irregularly shaped (e.g., skeletal or resorbed) spinels, indicating late-stage mineral reactions. Volatile bearing accessory minerals such as phlogopite, amphibole and apatite are common in Yangyuan Fe-rich peridotites. Clinopyroxenes from these Fe-rich peridotites have high REE concentrations, with La content up to 67 times the chondritic value, and convex-upward trace element patterns (Zhao et al., 2015). They also have extremely light Fe isotopes, with bulk rock $\delta^{57/54}$Fe as low as −0.64, among the lowest ever reported for terrestrial silicate rocks (Fig. 1). For comparison, most published $\delta^{57/54}$Fe values of global peridotites range from −0.1 to +0.1 (Fig. 1; Weyer and Ionov, 2007; Zhao et al., 2012, 2015; Craddock et al., 2013; Poitrasson et al., 2013), with a suggested $\delta^{57/54}$Fe value of 0.04 ± 0.04 for the upper mantle (Weyer and Ionov, 2007; Craddock et al., 2013).

In this study, three magnesium-peridotites and five Fe-rich peridotites, which have been studied by Zhao et al. (2015) for geochemical and Fe isotopic compositions, were selected for Ca isotopic analyses.

3. ANALYTICAL METHODS

Calcium isotope analyses were performed at the State Key Laboratory of Isotope Geochemistry, Guangzhou Institute of Geochemistry (GIG), Chinese Academy of Sciences. Detailed analytical procedures, including sample dissolution, column chemistry and instrumental analysis, are similar to that reported in Zhu et al. (2016) and Kang et al. (2016). About 2–30 mg of 200 mesh whole rock or mineral (orthopyroxene and clinopyroxene) powders were dissolved using 5:1 mixture of concentrated HF and HNO_3 in 7-ml Teflon beakers on a hot plate at 120 °C for a week. Then the sample solution was dried down twice with several drops of aqua regia at 80–90 °C, and twice with concentrated HCl. The sample was then dissolved in 1.6 N HCl for Ca column chemistry. An aliquot of sample solution containing ~50 μg Ca was mixed with a certain amount of ^{42}Ca-^{43}Ca double spike solution in a pre-cleaned PFA beaker. The spiked sample solution was dried down and re-dissolved in 0.1 ml 1.6 N HCl for column chemistry. Ca was purified using a Teflon micro-column filled with 1 ml cation exchange resin BioRad AG-MP50 (100–200 mesh) following the procedure described in Kang et al. (2016) and Zhu et al. (2016). Clinopyroxene solutions were passed through the column once, and whole rock and orthopyroxene solutions twice. At least two reference materials were processed as unknown samples for each batch of column chemistry to access accuracy and reproducibility. The column chemistry has been carefully calibrated to ensure a ~100% Ca recovery. The total procedure blank is 30–70 ng, which is only about 0.1–0.2% of the Ca used for each TIMS measurement.

Calcium isotopes were measured on a ThermoTriton™ thermal ionization mass-spectrometer hosted at GIG. A single sequence was used in which ^{40}Ca, ^{41}K, ^{42}Ca, ^{43}Ca and ^{44}Ca were collected in L2, C, H1, H2 and H3 Faraday cups, respectively. Possible isobaric interferences were carefully checked before data collection. ^{40}K interference on ^{40}Ca was corrected using $^{40}K/^{41}K = 1.7384 \times 10^{-3}$, and the correction is typically less than 0.01 δ units, which is negligible compared to our typical analytical precision. Double spike data reduction follows an iterative algorithm similar to Heuser et al. (2002) with the exponential fractionation law. Results are reported using $\delta^{44/40}$Ca relative to NIST SRM 915a, defined as $\delta^{44/40}Ca = [(^{44}Ca/^{40}Ca)_{sample}/(^{44}Ca/^{40}Ca)_{SRM915a} - 1] \times 1000$. Each sample has been measured multiple times using the same purified Ca cut, and the two standard deviation is reported as the analytical uncertainty. During the period of analysis, NIST SRM 915a and IAPSO seawater were routinely measured to monitor instrumental stability and reproducibility. The long-term average $\delta^{44/40}$Ca of SRM 915a and seawater are 0.02 ± 0.13 ($n = 18$, 2SD) and 1.83 ± 0.11 ($n = 11$, 2SD), respectively (Table 1), agreeing well with published values (DePaolo, 2004; Huang et al., 2010a; Valdes et al., 2014; Fantle and Tipper, 2014; Zhu et al., 2016; Kang et al., 2016; He et al., 2016). One sample (clinopyroxene separate of YY09-28) was replicated by digestion of a different mineral separate aliquot, and the measured Ca isotopic compositions agree within uncertainty (Table 1).

Our ^{42}Ca-^{43}Ca double spike technique only measures the ^{44}Ca/^{40}Ca variation, which is a combination of stable isotopic fractionation effect and radiogenic ^{40}Ca ingrowth from ^{40}K in terrestrial samples. In order to document possible radiogenic ^{40}Ca contribution, we also measured the unspiked Ca isotopic compositions in clinopyroxene and orthopyroxene separates from samples YY09-05 and YY09-28. The procedure of unspiked measurement is similar to that of spiked measurement, except that the sample solution was not mixed with a double spike solution. The instrumental mass bias is corrected to ^{42}Ca/^{44}Ca = 0.31221 using the exponential fractionation law.

4. RESULTS

Calcium isotopic compositions of reference materials, Yangyuan peridotite mineral separates and whole rocks are reported in Table 1. Some whole-rock Ca isotopic compositions are direct measurements, and others are calculated using the measured mineral Ca isotopic compositions and their mineral modal abundances (Table 1). The measured whole rock $\delta^{44/40}$Ca in general agree well with the calculated values. There are large $\delta^{44/40}$Ca variations in these peridotitic xenoliths. Mg-peridotites have $\delta^{44/40}$Ca similar to typical upper mantle value (Simon and DePaolo, 2010; Huang et al., 2010a; Valdes et al., 2014; Kang et al., 2016). Specifically, Mg-peridotite orthopyroxenes have $\delta^{44/40}$Ca ranging from 0.88 to 1.01 with an average of 0.93 ± 0.14 (2SD, $n = 3$), and Mg-peridotite clinopyroxenes have $\delta^{44/40}$Ca from 0.86 to 0.92 with an average of 0.89 ± 0.16 (2SD, $n = 3$) (Table 1 and Fig. 1). In contrast, $\delta^{44/40}$Ca in Fe-rich peridotites are highly variable and trend to extremely low values. Their clinopyroxenes have $\delta^{44/40}$Ca ranging from −0.09 to 0.69, and their orthopyroxenes have

Table 1
Calcium and iron isotopic compositions of Yangyuan peridotitic xenoliths and reference materials.[a]

Sample	Rock type	Mineral	$\delta^{44/40}$Ca	*n*	2SD	Sample	Mineral	$\delta^{57/54}$Fe	*n*	2SD	Mg#
YY09-47	Mg-peridotite	WR^C	0.86		0.13	YY09-47	WR^M	0.16	3	0.03	90.5
		Cpx	0.86	3	0.12		Ol	0.13	3	0.05	90.4
		Opx	0.90	3	0.04		Opx	0.16	3	0.04	91.0
YY11-06	Mg-peridotite	WR^C	0.89		0.09	YY11-06	WR^M	0.04	3	0.02	90.3
		Cpx	0.88	3	0.06		Ol	0.01	3	0.06	90.3
		Opx	1.01	3	0.06		Opx	0.07	3	0.04	90.7
YY09-07	Mg-peridotite	WR^C	0.92		0.09	YY09-07	WR^M	0.11	3	0.01	90.9
		Cpx	0.92	4	0.03		Ol	0.07	3	0.02	90.8
		Opx	0.88	3	0.09		Opx	0.11	3	0.04	91.3
YY09-05	Fe-rich peridotite	WR^C	−0.08		0.07	YY09-05	WR^M	−0.61	4	0.06	83.7
		WR^M	0.09	3	0.14		Ol	−0.62	4	0.07	82.2
		Cpx	−0.09	3	0.07		Opx	−0.10	4	0.01	86.3
		Opx	0.22	3	0.02						
YY09-28	Fe-rich peridotite	WR^C	0.22		0.10	YY09-28	WR^M	−0.62	4	0.03	80.1
		WR^M	0.24	3	0.14		Ol	−0.64	12	0.03	80.0
		Cpx	0.25	6	0.07		Opx	−0.12	4	0.01	83.3
		Replicate[b]	0.24	3	0.06						
		Opx	−0.24	4	0.06						
YY09-24	Fe-rich peridotite	WR^C	0.58		0.09	YY09-24	WR^M	−0.36	6	0.04	87.5
		Cpx	0.58	3	0.07		Ol	−0.36	6	0.05	87.7
		Opx	0.44	4	0.06		Opx	−0.97	12	0.02	88.1
YY09-18	Fe-rich peridotite	WR^C	0.66		0.06	YY09-18	WR^M	−0.40	4	0.04	86.6
		Cpx	0.67	3	0.05		Ol	−0.41	4	0.02	86.4
		Opx	0.59	3	0.03		Opx	−0.17	4	0.05	86.9
YY09-27	Fe-rich peridotite	WR^C	0.70		0.09	YY09-27	WR^M	−0.41	4	0.04	85.6
		Cpx	0.69	3	0.08		Ol	−0.41	4	0.05	85.8
		Opx	0.70	3	0.06		Opx	−0.26	12	0.02	86.7
Average host basalts			0.63	5	0.06	Average host basalts		0.26	5	0.03	
IAPSO seawater			1.83	11	0.11						
SRM 915a			0.02	18	0.13						

Sample	Rock type	Mineral	$(^{40}Ca/^{44}Ca)_N$[c]	*n*	2SD
YY09-05	Fe-rich peridotite	Cpx unspiked	47.159	1	0.12
		Replicate[b]	47.160	1	0.12
		Opx unspiked	47.160	1	0.12
YY09-28	Fe-rich peridotite	Cpx unspiked	47.159	1	0.12
		Opx unspiked	47.156	1	0.12
	915a	Unspiked	47.162	40	0.12

[a] WR, whole rock; Ol, olvine; Opx, orthopyroxene; Cpx, clinopyroxene; C, Calculated bulk $\delta^{44/40}$Ca based on mineral separate data and mineral mode from Zhao et al. (2015); M, Measured bulk $\delta^{44/40}$Ca and $\delta^{57/54}$Fe. Iron isotope and major element data are from Zhao et al. (2015).

[b] Replicate: Re-analysis from chemical separation to isotopic analysis, starting from the new digestion of same sample powder.

[c] Subscribe N represents internal normalization to $^{42}Ca/^{44}Ca = 0.31221$. Each sample has been analyzed once for unspiked measurement; consequently, the external reproducibility obtained by 40 measurements of NIST SRM 915a, ±0.012, is used as the analytical error for each single unspiked measurement.

$\delta^{44/40}$Ca ranging from −0.24 to 0.70 (Table 1 and Fig. 1). The lowest $\delta^{44/40}$Ca values are found in YY09-05 clinopyroxene (−0.09) and YY09-28 orthopyroxene (−0.24). They are the lowest $\delta^{44/40}$Ca ever reported for terrestrial silicate rocks and minerals (Fig. 1). More importantly, bulk rock Yangyuan peridotites show ~1‰ ^{44}Ca/^{40}Ca variation (e.g., $\delta^{44/40}$Ca = −0.08 to 0.92), which comprises over 30% variation of global carbonates (Fantle and Tipper, 2014), and 50% of that in global silicates (Fig. 1). The low $\delta^{44/40}$Ca values do not represent excess radiogenic ^{40}Ca ingrowth. This has been confirmed by our unspiked Ca isotopic measurements on clinopyroxene and orthopyroxene separates from YY09-05 and YY09-28, two with the lowest $\delta^{44/40}$Ca of −0.09 and −0.24. They have $(^{40}Ca/^{44}Ca)_N$ of 47.156–47.160, where subscript N represents value after internal normalization to $^{42}Ca/^{44}Ca = 0.31221$, which are indistinguishable from our unspiked measurement of NIST SRM 915a (47.162 ± 0.012, 2σ) (Table 1). Consequently, the measured $\delta^{44/40}$Ca variation in Yangyuan peridotites reflects mass-dependent isotopic variation.

5. DISCUSSION

5.1. Inter-mineral Ca isotopic fractionation in Yangyuan peridotites

In addition to their large $\delta^{44/40}$Ca variation, Yangyuan peridotites also show very unusual inter-mineral Ca isotopic fractionation between clinopyroxene and orthpyroxene. Since the heavier Ca isotopes favor the shorter and stiffer bonds of orthopyroxene (Feng et al., 2014), equilibrium inter-mineral isotopic fractionation $\Delta^{44/40}Ca^{OPX\text{-}CPX}$, defined as $\delta^{44/40}Ca^{OPX}$–$\delta^{44/40}Ca^{CPX}$, are positive (Huang et al., 2010a; Kang et al., 2016). Surprisingly, some Yangyuan Fe-rich peridotites have $\Delta^{44/40}Ca^{OPX\text{-}CPX}$ less than zero (Fig. 2). Together with published data, we find that $\Delta^{44/40}Ca^{OPX\text{-}CPX}$ is positively correlated with the Ca/(Ca + Mg + Fe) ratio in clinopyroxene, with R^2 of 0.64 (Fig. 2b). Ca/(Ca + Mg + Fe) ratios in studied clinopyroxene-orthopyroxene pairs are highly negatively correlated with each other (Fig. 2a), implying chemical equilibrium. Equilibrium temperature inferred using Ca-in-orthopyroxene thermometer (Brey and Köhler, 1990) is correlated with $\Delta^{44/40}Ca^{OPX\text{-}CPX}$ (Fig. 2c). However, it is unlikely that the large $\Delta^{44/40}Ca^{OPX\text{-}CPX}$ variation reflects a temperature effect, because $\Delta^{44/40}Ca^{OPX\text{-}CPX}$ ranges from negative to positive values. First principles calculation in a Fe-free system showed that $\Delta^{44/40}Ca^{OPX\text{-}CPX}$ is dependent on the chemical composition of orthopyroxene (Ca/Mg ratio) (Feng et al., 2014). Although the positive $\Delta^{44/40}Ca^{OPX\text{-}CPX}$ vs. $Ca/(Ca + Mg + Fe)_{CPX}$ trend (Fig. 2) may hint a compositional dependence of inter-mineral Ca isotopic fractionation, its detailed origin needs further investigation.

5.2. Origin of the coupled light Ca-Fe isotopic compositions in Yangyuan peridotites

5.2.1. Observations

Yangyuan Fe-rich peridotites are characterized by the lowest Mg#, the lowest $\delta^{57/54}$Fe, and the lowest $\delta^{44/40}$Ca among global peridotites (Fig. 1). Within Yangyuan peridotites, $\delta^{44/40}$Ca and $\delta^{57/54}$Fe are positively correlated with each other (Fig. 3). Their host basalts have $\delta^{44/40}$Ca of 0.63 and $\delta^{57/54}$Fe of 0.26 (Table 1), which are significantly higher than the lowest $\delta^{44/40}$Ca and $\delta^{57/54}$Fe in Yangyuan Fe-rich peridotites. Further, mixing between a peridotite with typical upper mantle $\delta^{44/40}$Ca and $\delta^{57/54}$Fe values and Yangyuan host basalt leads to a negative $\delta^{44/40}$Ca vs. $\delta^{57/54}$Fe trend, inconsistent with the observed positive trend formed by Yangyuan peridotites (Fig. 3).

The low $\delta^{44/40}$Ca in terrestrial silicate rocks has been attributed to a role of ancient carbonate (Huang et al., 2011a). However, mixing lines between a peridotite and sediments or carbonatites with low $\delta^{44/40}$Ca and $\delta^{57/54}$Fe are highly curved and fail to reproduce the $\delta^{44/40}$Ca vs. $\delta^{57/54}$Fe trend formed by Yangyuan peridotites (Fig. 3). This is because sediments (Plank and Langmuir, 1998) and carbonatites (Jones et al., 2013) have Ca/Fe much higher than peridotites.

5.2.2. Model to be tested

Yangyuan peridotites form positive $\delta^{44/40}$Ca vs. $\delta^{57/54}$Fe and Mg/Fe vs. $\delta^{57/54}$Fe trends, which can be explained as

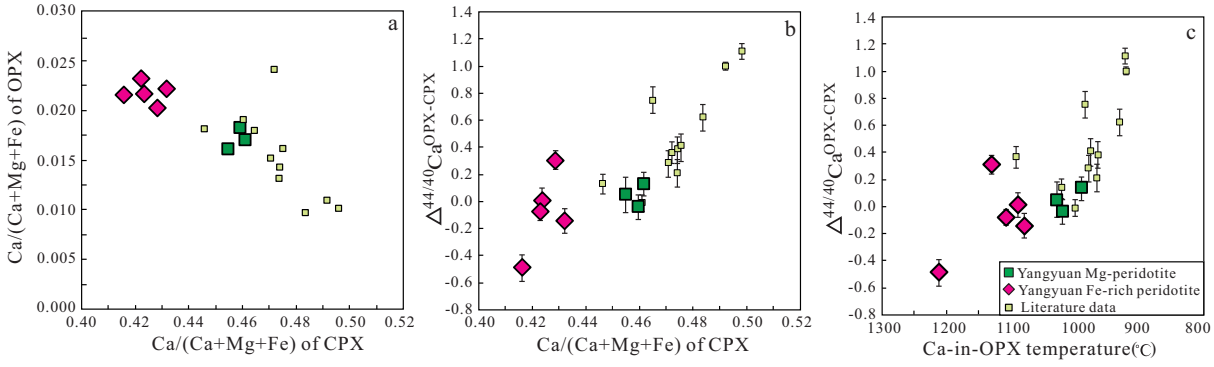

Fig. 2. Possible compositional effects on inter-mineral Ca isotopic fractionation. a, $Ca/(Ca + Mg + Fe)^{CPX}$ vs. $\Delta^{44/40}Ca^{OPX\text{-}CPX}$. b, $Ca/(Ca + Mg + Fe)^{OPX}$ vs. $\Delta^{44/40}Ca^{OPX\text{-}CPX}$. c, the correlation between equilibrium temperature calculated using Ca-in-orthopyroxene (Brey and Köhler, 1990) and $\Delta^{44/40}Ca^{OPX\text{-}CPX}$. The analytical uncertainty of $\Delta^{44/40}Ca^{OPX\text{-}CPX}$ is calculated by propagating the analytical errors on both clinopyroxene and orthopyroxene. Data are from Huang et al. (2010a), Kang et al. (2016), Zhao et al. (2015), and this study.

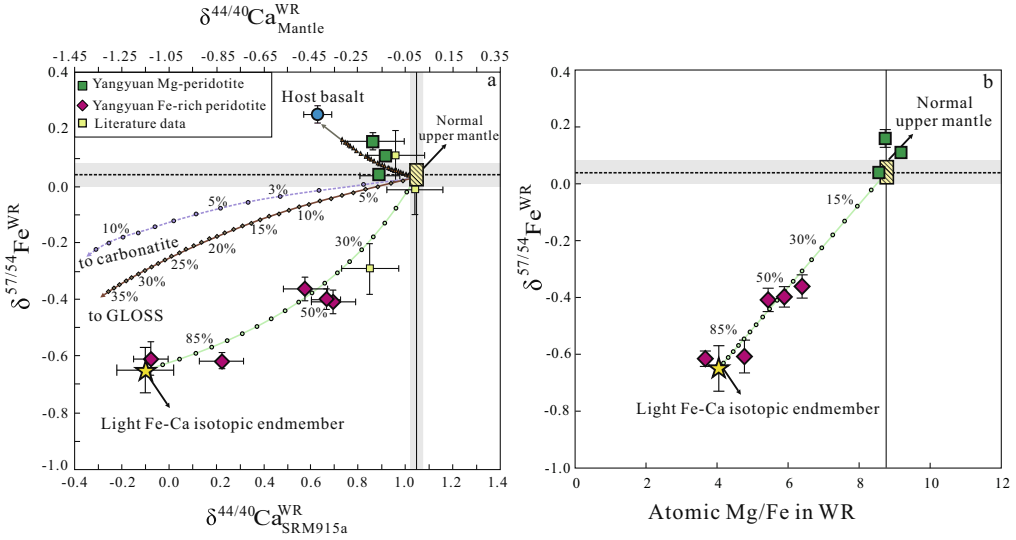

Fig. 3. (a) $\delta^{44/40}Ca$ vs. $\delta^{57/54}Fe$ and (b) Mg/Fe vs. $\delta^{57/54}Fe$ in bulk Yangyuan peridotites. Also shown is the host basalt for comparison. $\delta^{44/40}Ca$ data are from Table 1, and $\delta^{57/54}Fe$ data are from Zhao et al. (2015). Additional data are from Kang et al. (2016) and Huang et al. (2011b). The vertical solid line in panel (a) represents Ca isotopic composition of the upper mantle ($\delta^{44/40}Ca = 1.05 \pm 0.04$, Huang et al., 2010a), and the horizontal dashed line in panel (a) represents the suggested Fe isotopic composition of the upper mantle ($\delta^{57/54}Fe = 0.04 \pm 0.04$, Weyer and Ionov, 2007; Craddock et al., 2013). The vertical line in panel (b) shows the upper mantle Mg/Fe of 8.8 (McDonough, 1990). Three mixing lines of normal upper mantle with a sedimentary component (GLOSS, Plank and Langmuir, 1998), a carbonatite (Jones et al., 2013) and a reacted peridotite with light Ca-Fe isotopic compositions are shown in panel (a). The mixing lines between normal upper mantle and a sedimentary component or a carbonatite are highly curved, inconsistent with the $\delta^{44/40}Ca$ vs. $\delta^{57/54}Fe$ trend of Yangyuan peridotites. Mixing of a normal upper mantle with the host basalt leads to a negative $\delta^{44/40}Ca$ vs. $\delta^{57/54}Fe$ correlation, also inconsistent with the positive trend of Yangyuan peridotites. Mixing between a typical upper mantle peridotite and a reacted peridotite with light Ca-Fe isotopic compositions (yellow star) and low Mg/Fe can reproduce the positive trends by Yangyuan peridotites. Model details are: [MgO] = 41.4 wt.%, [CaO] = 2.33 wt.%, [FeO] = 8.52 wt.%, $\delta^{44/40}Ca_{SRM915a} = 1.05$ and $\delta^{57/54}Fe = 0.04$ for normal upper mantle (Weyer and Ionov, 2007; Huang et al., 2010a; Craddock et al., 2013; Zhao et al., 2015); [CaO] = 5.95 wt.%, [FeO] = 5.21 wt.%, $\delta^{44/40}Ca_{SRM915a} = -1.2$ and $\delta^{57/54}Fe = -1.6$ for sedimentary component (GLOSS) (Craddock et al., 2013; Fantle and Tipper, 2014); [CaO]= 28.9 wt.%, [FeO] = 11.5 wt.%, $\delta^{44/40}Ca_{SRM915a} = -1.2$ and $\delta^{57/54}Fe = -1.6$ for ferrocarbonatite (Plank and Langmuir, 1998; Huang et al., 2011b; Jones et al., 2013); [CaO] = 7.0 wt.%, [FeO] = 11.1 wt.%, $\delta^{44/40}Ca_{SRM915a} = 0.63$ and $\delta^{57/54}Fe = 0.26$ for Yangyuan host basalt (Ma and Xu, 2004 and Table 1) and [MgO] = 36 wt.%, [CaO] = 1.8 wt.%, [FeO] = 16 wt.%, $\delta^{44/40}Ca_{SRM915a} = -0.1$ and $\delta^{57/54}Fe = -0.65$ for the reacted peridotite with light Ca-Fe isotopic compositions (yellow star). (For interpretation of the references to colour in this figure legend, the reader is referred to the web version of this article.)

mixing lines between a normal upper mantle and a peridotite with low $\delta^{44/40}Ca$, $\delta^{57/54}Fe$ and Mg/Fe (Fig. 3). What caused the distinctive geochemical and isotopic signatures in Yangyuan peridotites (Fig. 3)? Here we propose that Yangyuan Fe-rich peridotites were generated by melt-peridotite reaction, and their extremely low $\delta^{57/54}Fe$ and $\delta^{44/40}Ca$ reflect kinetic isotopic effect during this melt-peridotite reaction (Fig. 4; Ionov et al., 2005; Xiao et al., 2013; Zhao et al., 2015). Yangyuan Fe-rich peridotites with Mg# ranging from 80.1 to 87.5 are metasomatized: their clinopyroxenes have convex-upward trace element patterns, and they contain accessory minerals such as phlogopite, amphibole and apatite (Zhao et al., 2015). Importantly, their Mg#s are significantly lower than the typical upper mantle value. They also display different stages of orthopyroxene replacement indicating late-stage melt-mineral reactions: some orthopyroxene grains have clinopyroxene rims with a sieve-texture, and some orthopyroxene relic cores are surrounded by newly formed sieve-textured clinopyroxene and irregularly shaped spinels (Fig. 4). Such replacement led to a higher ratio of clinopyroxene/orthopyroxene in the Yangyuan Fe-rich peridotites (0.7–1.3) than in the Mg-peridotites (0.3–0.5) (Zhao et al., 2015). These petrological and petrographic characteristics of Yangyuan Fe-rich peridotites are similar to that observed in Fe-rich peridotites from Tok, SE Siberia craton (Ionov et al., 2005). The petrogenesis of these Siberian Fe-rich peridotites involves reaction between refractory residual peridotite and a percolating melt (Ionov et al., 2005). Specifically, we propose that at Yangyuan orthopyroxene reacts with SiO_2-poor basaltic melt to form clinopyroxene, and high Fo olivine reacts with Fe-rich basaltic melt to form low Fo olivine (Fig. 4):

Melt 1 (high-Ca, high-Fe) + orthopyroxene
+ olivine (high Fo) → Melt2 (low-CaO, low-Fe)
+ clinopyroxene + olivine (low Fo) (ReactionI)

Two diffusion processes control this reaction: Fe in the melt diffuses into high-Fo olivine and Mg in high-Fo olivine diffuses outward to melt to make low-Fo olivine (Reaction II), and Ca in the melt diffuses into orthopyroxene to convert an orthopyroxene to clinopyroxene (Reaction III).

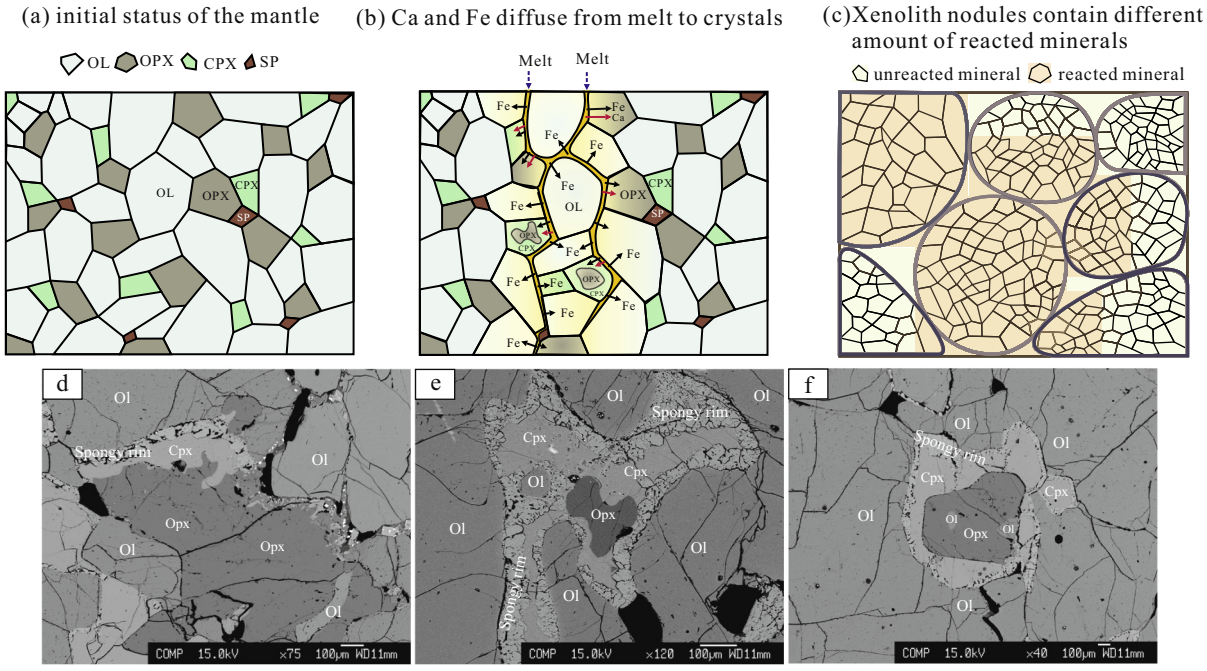

Fig. 4. An illustration of the element diffusion during a melt percolating through a peridotite. a, Initial condition of the peridotite. b, Ca and Fe diffuse from percolating melt into peridotite minerals, convert orthopyroxene to clinoproxene, and decrease the olivine Fo number. Black arrow indicates Fe diffusion and red arrow indicates Ca diffusion. Panel (c) is a cartoon to show that some xenolith nodules contain more reacted minerals, hence lighter Ca and Fe isotopic compositions, than others. These nodules may be re-homogenized by a later heating event(s), so that their minerals may reach equilibrium at hand specimen scale. d-f, Back-scattered electron images of Yangyuan Fe-rich peridotites, which show different stages of orthopyroxene replacement ranging from nearly intact orthopyroxene grains with rare sieve-textured clinopyroxene at rims to resorbed orthopyroxene relics inside newly formed sieve-textured clinopyroxene. (For interpretation of the references to colour in this figure legend, the reader is referred to the web version of this article.)

$$\text{Melt 1(high-Ca, high-Fe)} + \text{olivine (high Fo)} \rightarrow \text{Melt2 (low-CaO, low-Fe)} + \text{olivine (low Fo)} \quad \text{(ReactionII)}$$

$$\text{Melt 1(high-Ca, high-Fe)} + \text{orthopyroxene} \rightarrow \text{Melt 2 (low-CaO, low-Fe)} + \text{clinopyroxene} \quad \text{(ReactionIII)}$$

Diffusion reaction II is supported by the observation of distinctly lower Fo (80.0–87.7) in olivines from the Fe-rich peridotites, and Diffusion reaction III is supported by the observation of different stages of orthopyroxene replacement described above (Fig. 4). These two diffusion reactions would introduce kinetic isotopic fractionations of Ca and Fe, and their effects can be modeled (see next section). Weyer and Ionov (2007) and Poitrasson et al. (2013) have discussed the Fe isotopic effect during melt-peridotite reactions. In the first type of reaction (E1) of Weyer and Ionov (2007), a CaO-rich, SiO_2-poor melt reacts with peridotite, replaces orthopyroxene with clinopyroxene, and decreases Mg# of the peridotite. This chemical reaction is the same as our chemical reaction (Reaction I). However, E1 type reaction reaches isotopic equilibrium between melt and mineral phases (Weyer and Ionov, 2007); consequently, there is no kinetic isotopic effect. The isotopic variation produced during E1 type reaction results from the isotopic difference between refractory residual and reacting melt. The mixing model lines with carbonatite and sediment in Fig. 3 are in fact similar to E1 type reaction discussed in Weyer and Ionov (2007).

Our melt-peridotite reaction models (Fig. 4) are similar to E2 type melt-peridotite reaction of Weyer and Ionov (2007) and that discussed by Poitrasson et al. (2013). In detail, the melt-peridotite reaction does not reach isotopic equilibrium between melt and mineral phases, and the kinetic isotopic effect caused by element diffusion generates large isotopic variations in the reacted peridotites. Such melt-peridotite reaction actually is a common process during mantle metasomatism (Frey and Green, 1974), which plays an important role in generating mantle heterogeneity (Cooper et al., 2004; Workman et al., 2004; Le Roux et al., 2007).

The positive $\delta^{44/40}$Ca vs. $\delta^{57/54}$Fe and Mg/Fe vs. $\delta^{57/54}$Fe trends of Yangyuan peridotites are interpreted as mixing lines between a normal upper mantle and a reacted peridoitite (Fig. 3). So that $\delta^{44/40}$Ca and $\delta^{57/54}$Fe variations in Yangyuan peridotites reflect variable amounts of reacted olivine and pyroxene in each nodule, and the one containing more reacted minerals has lower $\delta^{44/40}$Ca and $\delta^{57/54}$Fe (Fig. 4c). Our goal is to understand the petrogenesis of the endmember with the lowest $\delta^{44/40}$Ca, $\delta^{57/54}$Fe and Mg/Fe (yellow star in Fig. 3). Within Yangyuan peridotites, olivine dominates the whole rock $\delta^{57/54}$Fe and Fe/Mg, and clinopyroxene dominates the whole rock $\delta^{44/40}$Ca (Fig. 5). Consequently, we focus on the olivine $\delta^{57/54}$Fe and clinopyroxene $\delta^{44/40}$Ca in following discussion.

5.2.3. Model calculations

Kinetic isotopic fractionation caused by diffusion has been experimentally demonstrated (Richter et al., 2009; Huang et al., 2010b) and observed in a variety of natural systems (Weyer and Ionov, 2007; Dauphas et al., 2010; Teng et al., 2011; Poitrasson et al., 2013; Sio et al., 2013; Zambardi et al., 2014; Lai et al., 2015; Oeser et al., 2015; Sio and Dauphas, 2017). Here we follow the approach described in Lai et al. (2015), adopted from Crank (1975), to model the geochemical and the kinetic isotopic effects in the two diffusion reactions described above. Specifically, Eq. (5) of Lai et al. (2015) is used to calculate diffusive effects on Ca and Fe isotopes. For simplicity, in our model calculation, all minerals of interest, pyroxenes and olivine, are treated as spheres. If the percolating melt flow rate and the melt/peridotite ratio are sufficiently high, the percolating melt composition does not vary with time. Following Crank (1975), after time t, the average element composition of a given mineral, $C(t)$, is:

$$C(t) = Ci + \frac{6(Ci - Cr)}{\pi^2}\sum_{n=1}^{\infty}\frac{1}{n^2}\exp\left(\frac{-Dtn^2\pi^2}{a^2}\right)$$

where Cr is the mineral composition that is in equilibrium with the percolating melt; Ci is its initial mineral composition before reaction; a is the radius of the mineral grain; and D is the diffusion coefficient of the element of interest in this particular mineral.

Isotopes are fractionated during diffusion process due to their slightly different diffusion coefficients (Richter et al., 2009; Huang et al., 2010b; Watkins et al., 2017). In particular, for two isotopes, i and j, of one element, the ratio of their diffusion coefficients is:

$$\frac{D_i}{D_j} = \left(\frac{m_j}{m_i}\right)^{\beta}$$

where m_i and m_j are their atomic masses and β is an empirical constant.

Using the approach described above, we model the Ca and Fe isotopic effects during the two diffusion processes: Fe in the percolating melt diffuses into high Fo olivine to form low Fo olivine (Reaction II), and Ca in the percolating melt diffuses into orthopyroxene to form clinopyroxene (Reaction III).

The olivine Fe isotopic compositions are function of its initial FeO content (Ci), the olivine FeO content that is in equilibrium with the percolating melt (Cr), the dimensionless parameter (Dt/a^2), and β_{Fe} in olivine. In our approach, we fix the initial olivine composition at Fo = 91, and let the percolating melt composition vary so that the corresponding equilibrium olivine compositions have Fo of 60, 70, 74, 78, 82, 86, and 90. In our model calculation, we do not consider the possible equilibrium Fe isotopic fractionation between basaltic melt and olivine (Teng et al., 2008), because it is too small compared to the Fe isotopic variations observed in Yangyuan peridotites (Fig. 1). Richter et al. (2009) experimentally determined β_{Fe} in basaltic melt to be 0.03. However, to the best of our knowledge, β_{Fe} in olivine has not been determined experimentally. It has been inferred based on isotopic zoning in natural olivines to be 0.05–0.30 (Teng et al., 2008; Sio et al., 2013; Oeser et al., 2015; Sio and Dauphas, 2017). In our model calculation, we let β_{Fe} in olivine vary as 0.05, 0.15, and 0.30. Our model results of Fe isotopic effect in olivines are shown in Fig. 6, plotted as a function of olivine Fo. Each thick line represents the modeled olivine $\delta^{57/54}$Fe vs. Fo relationship for one percolating melt composition, and points on different thick lines with the same Dt/a^2 are connected with thin grey lines, with their corresponding Dt/a^2 labeled next to the tie lines.

Similarly, Ca isotopic effects in clipyroxenes are also controlled by their initial CaO content, the percolating melt composition, the dimensionless parameter (Dt/a^2), and β_{Ca} in pyroxene. In our model calculations, the initial CaO content (Ci) is taken as 1%, typical of orthopyroxenes. Since natural clinopyroxenes have limited CaO variations (e.g.,

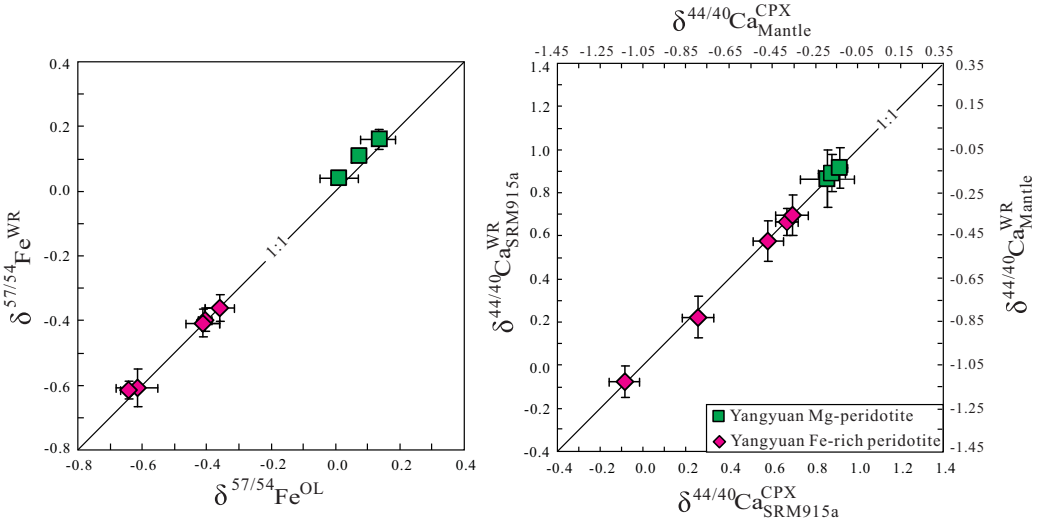

Fig. 5. Comparison of clinopyroxene $\delta^{44/40}$Ca with bulk rock $\delta^{44/40}$Ca, and olivine $\delta^{57/54}$Fe with bulk rock $\delta^{57/54}$Fe for Yangyuan peridotites. The near 1:1 correlations show that the bulk rock $\delta^{44/40}$Ca and $\delta^{57/54}$Fe are dominated by $\delta^{44/40}Ca^{CPX}$ and $\delta^{57/54}Fe^{OL}$, respectively, consistent with clinopyroxene being the dominant Ca-bearing phase and olivine being the dominant Fe-bearing phase in peridotites.

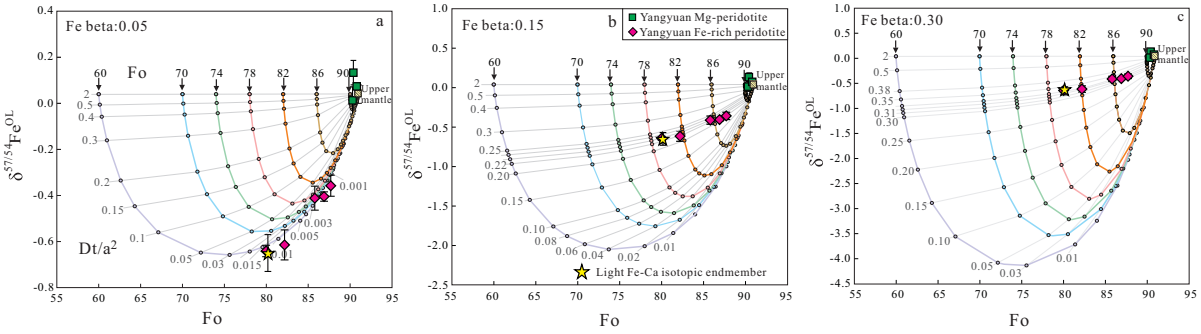

Fig. 6. Modeled results of Fe isotopic compositions and Fo numbers in olivines as a function of Dt/a^2 with three β_{Fe} values, 0.05, 0.15, and 0.30. Model details are given in the text. *Ci*, olivine initial composition, is fixed at 91, and *Cr* is varied as: 60, 70, 74, 78, 82, 86, and 90. The unreacted peridotites are characterized by typical upper mantle isotopic compositions, with $\delta^{57/54}Fe^{OL} = 0.04$. As shown in Fig. 5, the bulk peridotite $\delta^{57/54}Fe$ is dominated by $\delta^{57/54}Fe^{OL}$. Therefore, we focus on $\delta^{57/54}Fe^{OL}$ in this figure. Measured olivine Fo, $\delta^{57/54}Fe^{OL}$ and the proposed light Ca-Fe isotopic endmember (yellow star) are shown for comparison. Each thick line represents the modeled olivine $\delta^{57/54}Fe$ vs. Fo relationship for one percolating melt composition, and points on different thick lines with the same olivine Dt/a^2 are connected with thin grey lines, with their corresponding Dt/a^2 labeled next to the tie lines. (For interpretation of the references to colour in this figure legend, the reader is referred to the web version of this article.)

Leterrier et al., 1982), in our model calculations, clinopyroxenes that are in equilibrium with basaltic melts have 20% CaO, and do not vary with the percolating melt compositions. β_{Ca} in melts ranges from 0.04 to 0.2, but there is no direct measurement or indirect inference on clinopyroxene (see Watkins et al., 2017 for a summary). In our model calculation, we let β_{Ca} in clinopyroxene vary as 0.05, 0.075, and 0.10. The dimensionless parameter Dt/a^2 of pyroxene is related to that of olivine. Particularly, the olivine and pyroxene reaction times are the same. The diffusion coefficients of Fe in olivine and Ca in pyroxene are functions of temperature, and both olivine and pyroxene were under the same temperature during melt-peridotite reaction. Specifically, under a given temperature and a given (olivine: pyroxene) size ratio, each pyroxene Dt/a^2 is corresponding to one olivine Dt/a^2 value, and their relationship is shown in Fig. 7. Consequently, the Ca isotopic effect in clinopyroxene and the Fe isotopic effect in olivine generated through two diffusion reactions (Reactions II and III) are correlated with each other, and their relationship is shown in Fig. 8 and Supplemental Fig. 1. Thick lines in Fig. 8 and Supplemental Fig. 1 represent the modeled clinopyroxene $\delta^{44/40}Ca$ vs. olivine $\delta^{57/54}Fe$ relationship for different percolating melt compositions whose corresponding equilibrium olivine Fo are labeled next to them. Thin grey tie lines link points with the same olivine Dt/a^2 on different thick lines, with their corresponding Dt/a^2 labeled next to the tie lines.

5.2.4. Comparison of model calculation results and observations: constraints on melt-peridotite reaction conditions

In this section, we constrain the origin of the light Ca and Fe isotopic endmember in Yangyuan peridotites (yellow star in Fig. 3) using our model results presented in the previous section (Fig. 8 and Supplemental Fig. 1). Successful model results should explain the olivine Fo, olivine $\delta^{57/54}Fe$, and clinopyroxene $\delta^{44/40}Ca$ of the light Ca-Fe isotopic endmember at the same time. Here we explain how this works using β_{Fe} in olivine = 0.15 as an example. In Fig. 6b, olivine Fo and $\delta^{57/54}Fe$ of the light Ca-Fe isotopic endmember can be reproduced by a reaction between a typical upper mantle peridotite with a percolating melt whose equilibrium olivine Fo is 79 with the dimensionless parameter Dt/a^2 of 0.22–0.25. Fig. 8 is then used to evaluate whether the corresponding clinopyroxene $\delta^{44/40}Ca$ obtained from diffusion calculation matches that in the light Ca-Fe isotopic endmember clinopyroxene. We find that five combinations of olivine: pyroxene size ratio, temperature, and β_{Ca} in clinopyroxene can reproduce both clinopyroxene $\delta^{44/40}Ca$ and olivine $\delta^{57/54}Fe$ in the light Ca-Fe isotopic endmember (Fig. 8).

In our calculations, we have explored a limited parameter space, with β_{Fe} in olivine varying as 0.05, 0.15, and 0.30, β_{Ca} in clinopyroxene 0.05, 0.075, and 0.10, (olivine: pyroxene) size ratio 2:1, 1:1, and 1:2, and temperature 1000, 1100, and 1200 °C. Consequently, there are total 81 combinations of these parameters, and their modeled clinopyroxene $\delta^{44/40}Ca$ vs. olivine $\delta^{57/54}Fe$ relationship are shown in Supplemental Fig. 1, and the ones that are able to reproduce both clinopyroxene $\delta^{44/40}Ca$ and olivine $\delta^{57/54}Fe$ in the light Ca-Fe isotopic endmember are shown in Fig. 8. In summary, there are nine combinations in our explored parameter space (Table 2) that can reproduce olivine Fo, olivine $\delta^{57/54}Fe$, and clinopyroxene $\delta^{44/40}Ca$ of the light Ca-Fe isotopic endmember at the same time.

Within the combinations of model parameters that can reproduce the light Ca-Fe isotopic endmember, the required olivine Dt/a^2 varies from 0.01 to 0.35 according to different β_{Fe} in olivine. Clearly, β_{Fe} in olivine and β_{Ca} in clinopyroxene must be more precisely determined before melt-peridotite reaction conditions can be better constrained (Table 2). Nevertheless, melt-peridotite reaction time that is responsible to reproduce the light Ca-Fe isotopic endmember at Yangyuan can be estimated (Fig. 9). At Yangyuan, olivine radius size ranges from ~0.3 to 2 mm. Consequently, the estimated melt-peridotite reaction time ranges from 1–700 years for β_{Fe} in olivine of 0.05, to 15–16,000 years for β_{Fe} in olivine of 0.30.

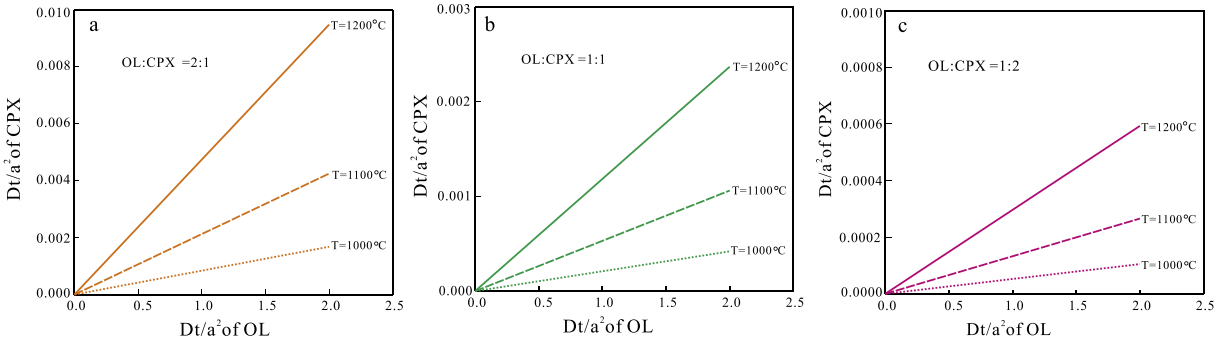

Fig. 7. Dt/a^2 of pyroxene and olivine as function of temperature and size ratio of pyroxene and olivine. Ca diffusion coefficient in clinpyoroxene is calculated using the equation from Brady and McCallister (1983), and Fe diffusion coefficient in olivine is from Chakraborty (1997).

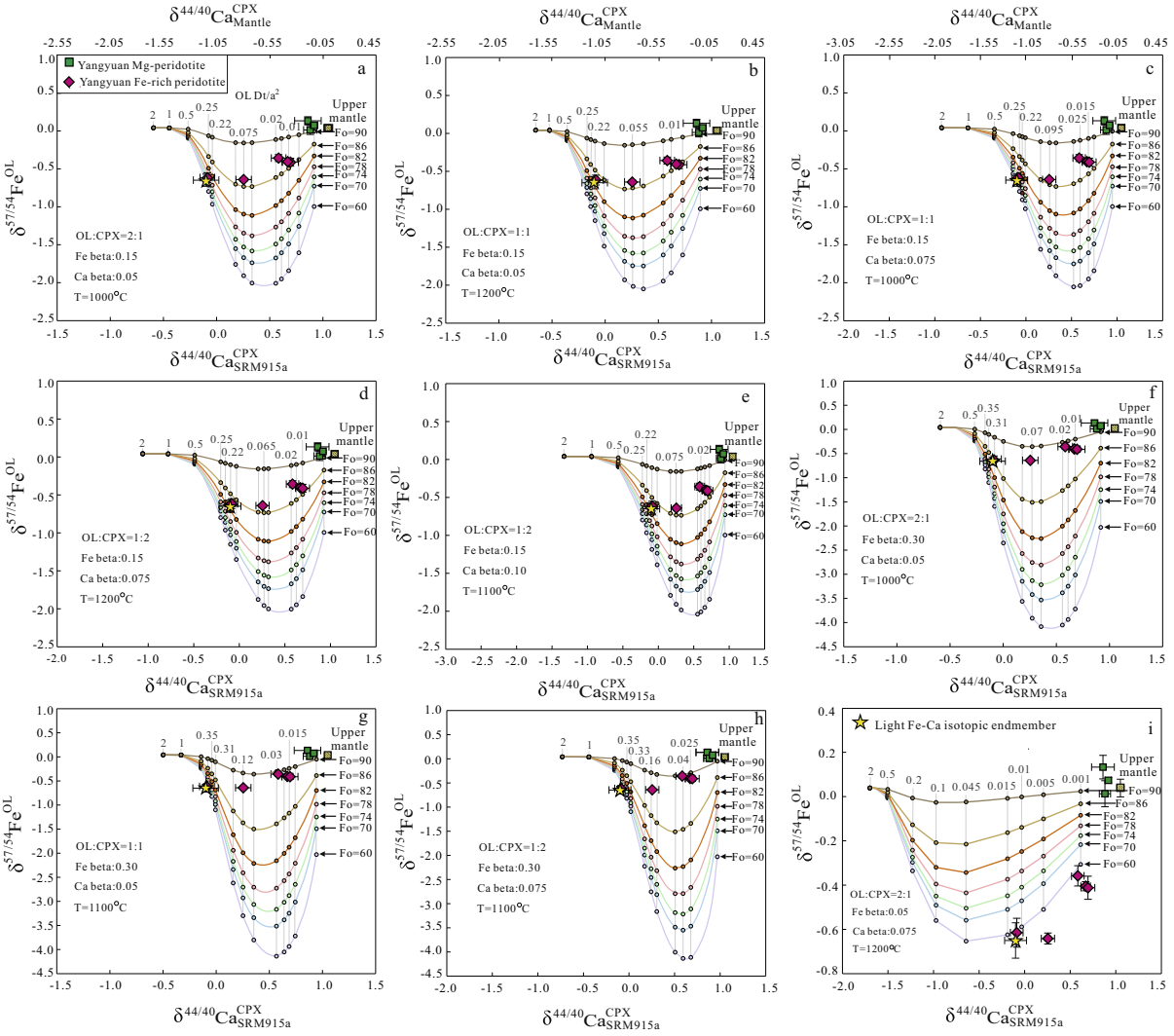

Fig. 8. Modeled covariations of $\delta^{44/40}Ca^{CPX}$ and $\delta^{57/54}Fe^{OL}$ introduced by diffusional fractionation. The combinations of β values, olivine: clinopyroxene size ratio, and temperatures that are able to reproduce the light Ca-Fe isotopic endmember at Yangyuan (yellow star, see Fig. 3) are shown, and the details are given in the legend. The Fe isotopic compositions of measured olivine and Ca isotopic compositions of measured clinopyroxene in Yangyuan peridotites are also shown for comparison.

Table 2
Combinations of parameters that can reproduce olivine Fo, olivine $\delta^{57/54}$Fe, and clinopyroxene $\delta^{44/40}$Ca of the light Ca-Fe isotopic endmember.

No.	β_{Fe} in olivine	β_{Ca} in clinopyroxene	Olivine: clinopyroxene size ratio	Temperature (°C)	Olivine Dt/a^2
1	0.05	0.075	2:1	1200	0.010–0.015
2	0.15	0.05	2:1	1000	0.22–0.25
3	0.15	0.05	1:1	1200	0.22–0.25
4	0.15	0.075	1:1	1000	0.22–0.25
5	0.15	0.075	1:2	1200	0.22–0.25
6	0.15	0.10	1:2	1100	0.22–0.25
7	0.30	0.05	2:1	1100	0.31–0.35
8	0.30	0.05	1:1	1100	0.31–0.35
9	0.30	0.075	1:2	1100	0.31–0.35

5.3. Comparison of the Mg# vs. $\delta^{57/54}$Fe correlations in Yangyuan peridotites vs. global peridodites and ureilites

Weyer and Ionov (2007) and Poitrasson et al. (2013) used a plot of Mg# vs. $\delta^{57/54}$Fe to show the effects of metasomatism and partial melting on peridotites. In such a plot, global peridotites show three trends: a horizontal trend, and two positive trends (Fig. 1c). The horizontal trend can be explained as a result of equilibrium metasomatism process, during which melt and peridotite reached isotopic equilibrium. The positive trend defined mostly by Yangyuan peridotites reflects the effect of an unequilibrated metasomatism process as discussed in Section 5.2. The steepest trend, with low-Mg# and -$\delta^{57/54}$Fe endmember defined by Beiyan Fe-rich peridotites (CLB samples, Fig. 1c; Zhao et al., 2012) may also reflect an unequilibrated metasomatism process, similar to what we proposed for Yangyuan peridotites. If so, these low-Mg# and -$\delta^{57/54}$Fe Beiyan Fe-rich peridotites should also be characterized by lighter Ca isotopic signatures; a prediction to be tested in future study. Alternatively, such trend could also reflect a mantle metasomatism effect involving an Fe-rich, low-$\delta^{57/54}$Fe melt, which may be a sulfide-rich magma, such as arc magmas that experienced extensive crystal fractionation (Lee et al., 2012), because sulfides tend to have lighter Fe isotopic signature due to the weak Fe-S bond (e.g., Wang et al., 2014).

Ureilites are a type of C-rich achondrites, which consist of mainly olivine and pyroxene, and represent the mantle rocks of one or a series of differentiated parent body or bodies (e.g., Goodrich, 1992). Ureilites show large Mg# variation, from 70 to 92 (Singletary and Grove, 2003), similar to our studied Yangyuan peridotites (Fig. 1c). However, ureilites form a horizontal Mg# vs. $\delta^{57/54}$Fe trend (Fig. 1c). Whether the large Mg# variation in ureilites was produced by the smelting process is being debated (Singletary and Grove, 2003, 2006; Warren, 2012). Barrat et al. (2015) found ureilites $\delta^{57/54}$Fe ranging from 0.03 to 0.21, slightly higher than average chondritic value (0.01 ± 0.01, see Fig. 3 of Craddock et al., 2013), and their $\delta^{57/54}$Fe are not correlated with their Mg# (Fig. 1c; Fig. 2 of Barrat et al., 2015). Barrat et al. (2015) argued that the high $\delta^{57/54}$Fe in ureilites were generated during early separation of Fe-FeS melts, which are characterized by low $\delta^{57/54}$Fe probably because of the weak Fe-S bond, from the ureilite parent body. However, this sulfur-rich Fe melt segregation model does not explain the lack of correlation between Mg# and $\delta^{57/54}$Fe in ureilites, leaving the large Mg# variation in ureilites to be explained by other processes. Smelting process is a type of melt-peridotite reaction, in which C-rich basaltic melt reacts with olivines to form pigeonites, metallic Fe and CO gas (Singletary and Grove, 2003, 2006). If melt and ureilites were in equilibrium, i.e., no kinetic isotopic effect, which is supported by the petrographic observation of ureilites (Singletary and Grove,

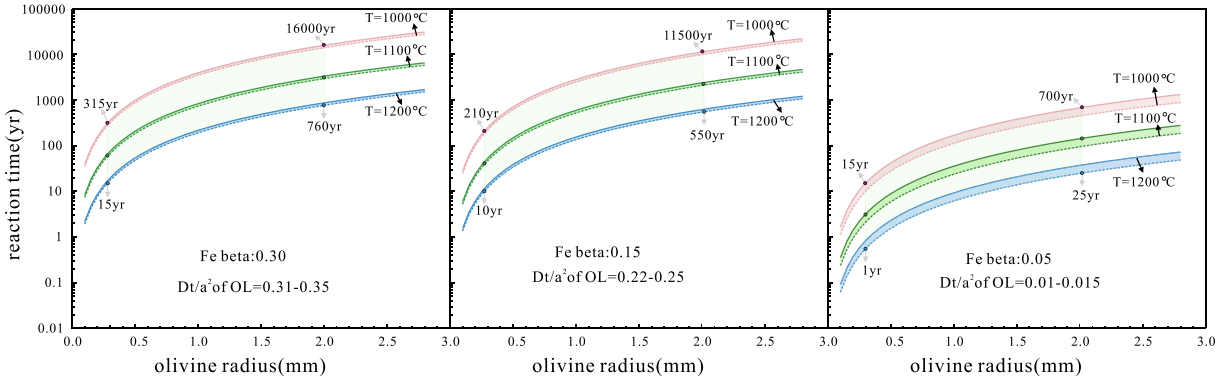

Fig. 9. Reaction time vs. the radius of olivine. The legend provides details of the β_{Fe} values, temperatures and Dt/a^2 of olivine that are able to reproduce the light Ca-Fe isotopic endmember at Yangyuan (yellow star, see Fig. 6). Possible olivine radius size range (from ~0.3 to 2 mm) of Yangyuan peridotites is labeled in each panel as green area. Fe diffusion coefficient in olivine is calculated using the equation from Chakraborty (1997). (For interpretation of the references to colour in this figure legend, the reader is referred to the web version of this article.)

2003), smelting model does predict a horizontal Mg# vs. $\delta^{57/54}$Fe trend for ureilites, because of the limited Fe isotopic fractionation between metallic Fe and silicates (Poitrasson et al., 2009). If this is the case, the high ureilite $\delta^{57/54}$Fe must be a primordial signature of ureilite parent body.

6. CONCLUSIONS

In conclusion, we found extremely large (~0.2‰ per amu) Ca and Fe isotopic variations within a set of North China Craton peridotites, and the lightest Ca-Fe isotopic signatures ever reported for terrestrial silicate rocks in a subset of Fe-rich peridotites. These distinctive isotopic signatures best reflect kinetic isotopic effects caused by diffusion during melt-peridotite reaction at a time scale of 1–10^4 years, depending on model details. This study clearly demonstrates that metal isotopic fractionation is a powerful tool studying magmtic/metamorphic processes occurred on a short time scale.

Together with published Ca isotopic data on clinopyroxene-orthopyroxene pairs, we show large inter-mineral Ca isotopic fractionation between clinopyroxene and orthopyroxene that is correlated with the major element compositions of both minerals. This correlation may infer a compositional effect on inter-mineral Ca isotopic fractionation between clinopyroxene and orthopyroxene; however, its detailed origin needs further investigation.

Both Yangyuan peridotites and ureilites show large Mg# variations; however, they form different Mg# vs. $\delta^{57/54}$Fe trends: a positive trend for Yangyuan peridotites and a horizontal trend for ureilites (Barrat et al., 2015), implying different origins for the large Mg# variations in these two suites of mantle rocks.

ACKNOWLEDGEMENTS

This work is supported by Natural Science Foundation of China (41673021, 41373007, 41373041, 41490632 and 91328204), State Key Laboratory of Lithospheric Evolution (Y610201102), State Key Laboratory of Isotope Geochemistry (SKLIG-KF-13-03), and National Science Foundation (EAR-1524387). We thank Guiqin Wang and Jinting Kang for help with Ca isotopic measurement, Jerry Wasserburg and Fred Frey for discussions and Editor Stefan Weyer, Martin Oeser, Paolo Sossi, and two anonymous reviewers for their helpful and constructive comments.

APPENDIX A. SUPPLEMENTARY MATERIAL

Supplementary data associated with this article can be found, in the online version, at http://dx.doi.org/10.1016/j.gca.2017.03.024.

REFERENCES

Barrat J. A., Rouxel O., Wang K., Moynier F., Yamaguchi A., Bischoff A. and Langlade J. (2015) Early stages of core segregation recorded by Fe isotopes in an asteroidal mantle. *Earth Planet. Sci. Lett.* **419**, 93–100.

Brady J. B. and McCallister R. H. (1983) Diffusion data for clinopyroxenes from homogenization and self-diffusion experiments. *Am. Mineral.* **68**, 95–105.

Brey G. P. and Köhler T. (1990) Geothermobarometry in four-phase lherzolites II: new thermo barometers, and practical assessment of existing thermobarometers. *J. Petrol.* **31**(6), 1353–1378.

Chakraborty S. (1997) Rates and mechanisms of Fe-Mg interdiffusion in olivine at 980 °C-1300°C. *J. Geophys. Res.* **102**, 12317–12331.

Clayton R. N., Hinton R. W. and Davis A. M. (1988) Isotopic variations in the rock-forming elements in meteorite. *Phil. Trans. R. Soc. Lond. A* **325**(1587), 483–501.

Cooper K. M., Eiler J. M., Asimow P. D. and Langmuir C. H. (2004) Oxygen isotope evidence for the origin of enriched mantle beneath the mid-Atlantic ridge. *Earth Planet. Sci. Lett.* **220**(3), 297–316.

Craddock P. R., Warren J. M. and Dauphas N. (2013) Abyssal peridotites reveal the near-chondritic Fe isotopic composition of the Earth. *Earth Planet. Sci. Lett.* **365**, 63–76.

Crank J. T. (1975) *The Mathematics of Diffusion*, second ed. Clarendon Press, Oxford.

Dauphas N., Teng F. Z. and Arndt N. T. (2010) Magnisium and iron isotopes in 2.7 Ga Alexo komatiites: Mantle signatures, no evidence for Soret diffusion, and identification of diffusive transport in zoned olivine. *Geochim. Cosmochim. Acta* **74**, 3274–3291.

DePaolo D. J. (2004) Calcium isotopic variations produced by biological, kinetic, radiogenic and nucleosynthetic processes. *Rev. Mineral. Geochem.* **55**, 255–288.

Fantle M. S. and Tipper E. T. (2014) Calcium isotopes in the global biogeochemical Ca cycle: implications for development of a Ca isotope proxy. *Earth Sci. Rev.* **129**, 148–177.

Feng C., Qin T., Huang S., Wu Z. and Huang F. (2014) First-principles investigations of equilibrium calcium isotope fractionation between clinopyroxene and Ca-doped orthopyroxene. *Geochim. Cosmochim. Acta* **143**, 132–142.

Frey F. A. and Green D. H. (1974) The mineralogy, geochemistry and origin of Iherzolite inclusions in Victorian basanites. *Geochim. Cosmochim. Acta* **38**, 1023–1059.

Goodrich C. A. (1992) Ureilites: a critical review. *Meteoritics* **27**, 327–352.

He Y., Wang Y., Zhu C., Huang S. and Li S. (2016) Mass-independent and mass-dependent Ca isotopic compositions of thirteen geological reference materials measured by thermal ionisation mass spectrometry. *Geostand. Geoanal. Res.*. http://dx.doi.org/10.1111/ggr.12153.

Heuser A., Eisenhauer A., Gussone N., Bock B., Hansen B. T. and Nägler T. F. (2002) Measurement of calcium isotopes (δ^{44}Ca) using a multicollector TIMS technique. *Int. J. Mass. Spectrom.* **220**(3), 385–397.

Huang S., Farkaš J. and Jacobsen S. B. (2010a) Calcium isotopic fractionation between clinopyroxene and orthopyroxene from mantle peridotites. *Earth Planet. Sci. Lett.* **292**, 337–344.

Huang F., Chakraborty P., Lundstrom C. C., Holmden C., Glessner J. J. G., Kieffer S. W. and Lesher C. E. (2010b) Isotope fractionation in silicate melts by thermal diffusion. *Nature* **464**(7287), 396–400.

Huang S., Farkaš J. and Jacobsen S. B. (2011a) Stable calcium isotopic compositions of Hawaiian shield lavas: evidence for recycling of ancient marine carbonates into the mantle. *Geochim. Cosmochim. Acta* **75**(17), 4987–4997.

Huang F., Zhang Z., Lundstrom C. C. and Zhi X. (2011b) Iron and magnesium isotopic compositions of peridotite xenoliths from Eastern China. *Geochim. Cosmochim. Acta* **75**(12), 3318–3334.

Huang S. and Jacobsen S. B. (2017) Calcium isotopic compositions of chondrites. *Geochim. Cosmochim. Acta* **201**, 364–376.

Ionov D. A., Chanefo I. and Bodinier J. L. (2005) Origin of Fe-rich lherzolites and wehrlites from Tok, SE Siberia by reactive melt

percolation in refractory mantle peridotites. *Contrib. Miner. Petrol.* **150**, 335–353.
Jones A. P., Genge M. and Carmod Y. L. (2013) Carbonate melts and carbonatites. *Rev. Mineral. Geochem.* **75**(1), 289–322.
Kang J. T., Zhu H. L., Liu Y. F., Liu F., Wu F., Hao Y. T., Zhang Z. F. and Huang F. (2016) Calcium isotopic composition of mantle xenoliths and minerals from Eastern China. *Geochim. Cosmochim. Acta* **174**, 335–344.
Lai Y. J., von Strandmann P. A. P., Dohmen R., Takazawa E. and Elliott T. (2015) The influence of melt infiltration on the Li and Mg isotopic composition of the Horoman Peridotite Massif. *Geochim. Cosmochim. Acta* **164**, 318–332.
Le Roux V., Bodinier J. L., Tommasi A., Alard O., Dautria J. M., Vauchez A. and Riches A. J. V. (2007) The Lherz spinel lherzolite: refertilized rather than pristine mantle. *Earth Planet. Sci. Lett.* **259**(3), 599–612.
Lee C. T. A., Luffi P., Chin E. J., Bouchet R., Dasgupta R., Morton D. M., Le Roux V., Yin Q. Z. and Jin D. (2012) Copper systematics in arc magmas and implications for crust-mantle differentiation. *Science* **336**(6077), 64–68.
Leterrier J., Maury R. C., Thonon P., Girard D. and Marchal M. (1982) Clinopyroxene composition as a method of identification of the magmatic affinities of paleo-volcanic series. *Earth Planet. Sci. Lett.* **59**(1), 139–154.
Liu R. X., Chen W. J., Sun J. Z. and Li D. M. (1992) The K-Ar age and tectonic environment of Cenozoic volcanic rock in China. In *The Age and Geochemistry of Cenozoic Volcanic Rock in China* (ed. R. X. Liu). Seismologic Press, Beijing, pp. 1–43 (in Chinese).
Ma J. L. and Xu Y. G. (2004) Petrology and geochemistry of the Cenozoic Basalts from Yangyuan of Hebei Province and Datong of Shanxi Province: implications for the deep process in the Western North China Craton. *Geochimica* **33**, 75–88.
McDonough W. F. (1990) Constraints on the composition of the continental lithospheric mantle. *Earth Planet. Sci. Lett.* **101**(1), 1–18.
Oeser M., Dohmen R., Horn I., Schuth S. and Weyer S. (2015) Processes and time scales of magmatic evolution as revealed by Fe–Mg chemical and isotopic zoning in natural olivines. *Geochim. Cosmochim. Acta* **154**, 130–150.
Plank T. and Langmuir C. H. (1998) The chemical composition of subducting sediment and its consequences for the crust and mantle. *Chem. Geol.* **145**(3), 325–394.
Poitrasson F., Roskosz M. and Corgne A. (2009) No iron isotope fractionation between molten alloys and silicate melt to 2000 C and 7.7 GPa: Experimental evidence and implications for planetary differentiation and accretion. *Earth Planet. Sci. Lett.* **278**(3), 376–385.
Poitrasson F., Delpech G. and Grégoire M. (2013) On the iron isotope heterogeneity of lithospheric mantle xenoliths: implications for mantle metasomatism, the origin of basalts and the iron isotope composition of the Earth. *Contrib. Miner. Petrol.* **165**(6), 1243–1258.
Richter F. M., Watson E. B., Mendybaev R., Dauphas N., Georg B., Watkins J. and Valley J. (2009) Isotopic fractionation of the major elements of molten basalt by chemical and thermal diffusion. *Geochim. Cosmochim. Acta* **73**(14), 4250–4263.
Simon J. I. and DePaolo D. J. (2010) Stable calcium isotopic composition of meteorites and rocky planets. *Earth Planet. Sci. Lett.* **289**, 457–466.
Singletary S. J. and Grove T. L. (2003) Early petrologic processes on the ureilite parent body. *Meteorit. Planet. Sci.* **38**, 95–108.
Singletary S. J. and Grove T. L. (2006) Experimental constraints on ureilite petrogenesis. *Geochim. Cosmochim. Acta* **70**, 1291–1308.
Sio C. K. I., Dauphas N., Teng F. Z., Chaussidon M., Helz R. T. and Roskosz M. (2013) Discerning crystal growth from diffusion profiles in zoned olivine by in situ Mg–Fe isotopic analyses. *Geochim. Cosmochim. Acta* **123**, 302–321.
Sio C. K. I. and Dauphas N. (2017) Thermal and crystallization histories of magmatic bodies by Monte Carlo inversion of Mg-Fe isotopic profiles in olivine. *Geology* **45**(1), 67–70.
Teng F. Z., Dauphas N. and Helz R. T. (2008) Iron isotope fractionation during magmatic differentiation in Kilauea Iki lava lake. *Science* **320**(5883), 1620–1622.
Teng F. Z., Dauphas N., Helz R. T., Gao S. and Huang S. (2011) Diffusion-driven magnesium and iron isotope fractionation in Hawaiian olivine. *Earth Planet. Sci. Lett.* **308**(3), 317–324.
Valdes M. C., Moreira M., Foriel J. and Moynier F. (2014) The nature of Earth's building blocks as revealed by calcium isotopes. *Earth Planet. Sci. Lett.* **394**, 135–145.
Wang K., Day J. M., Korotev R. L., Zeigler R. A. and Moynier F. (2014) Iron isotope fractionation during sulfide-rich felsic partial melting in early planetesimals. *Earth Planet. Sci. Lett.* **392**, 124–132.
Warren P. H. (2012) Parent body depth-pressure-temperature relationships and the style of ureilite anatexis. *Meteorit. Planet. Sci.* **47**, 209–227.
Watkins J. M., DePaolo D. J. and Watson E. B. (2017) Kinetic fractionation of non-traditional stable isotopes by diffusion and crystal growth reactions. *Rev. Mineral. Geochem.* **82**(1), 85–125.
Weyer S. and Ionov D. A. (2007) Partial melting and melt percolation in the mantle: the message from Fe isotopes. *Earth Planet. Sci. Lett.* **259**, 119–133.
Williams H. M. and Bizimis M. (2014) Iron isotope tracing of mantle heterogeneity within the source regions of oceanic basalts. *Earth Planet. Sci. Lett.* **404**, 396–407.
Workman R. K., Hart S. R., Jackson M., Regelous M., Farley K. A., Blusztajn J., Kurz M. and Staudigel H. (2004) Recycled metasomatized lithosphere as the origin of the Enriched Mantle II (EM2) end-member: Evidence from the Samoan Volcanic Chain. *Geochem. Geophys. Geosyst.* **5**(4).
Xiao Y., Teng F. Z., Zhang H. F. and Yang W. (2013) Large magnesium isotope fractionation in peridotite xenoliths from eastern North China craton: Product of melt–rock interaction. *Geochim. Cosmochim. Acta* **115**, 241–261.
Young E. D., Tonui E., Manning C. E., Schauble E. and Macris C. A. (2009) Spinel–olivine magnesium isotope thermometry in the mantle and implications for the Mg isotopic composition of Earth. *Earth Planet. Sci. Lett.* **288**(3), 524–533.
Young E. D., Manning C. E., Schauble E. A., Shahar A., Macris C. A., Lazar C. and Jordan M. (2015) High-temperature equilibrium isotope fractionation of non-traditional stable isotopes: Experiments, theory, and applications. *Chem. Geol.* **395**, 176–195.
Zambardi T., Lundstrom C. C., Li X. and McCurry M. (2014) Fe and Si isotope variations at Cedar Butte volcano; insight into magmatic differentiation. *Earth Planet. Sci. Lett.* **405**, 169–179.
Zhao X. M., Zhang H. F., Zhu X. K., Tang S. H. and Yan B. (2012) Iron isotope evidence for multistage melt–peridotite interactions in the lithospheric mantle of eastern China. *Chem. Geol.* **292**, 127–139.
Zhao X. M., Zhang H. F., Zhu X. K., Zhu B. and Cao H. H. (2015) Effects of melt percolation on iron isotopic variation in peridotites from Yangyuan, North China Craton. *Chem. Geol.* **401**, 96–110.
Zhong Y., Chen L. H., Wang X. J., Zhang G. L., Xie L. W. and Zeng G. (2017) Magnesium isotopic variation of oceanic island basalts generated by partial melting and crustal recycling. *Earth Planet. Sci. Lett.* **463**, 127–135.
Zhu H. L., Zhang Z. F., Wang G. Q., Liu Y. F., Liu F., Li X. and Sun W. D. (2016) Calcium Isotopic Fractionation during Ion - Exchange Column Chemistry and Thermal Ionisation Mass Spectrometry (TIMS) Determination. *Geostand. Geoanal. Res.* **40**, 185–194.

Associate editor: Stefan Weyer